

UCSF

UC San Francisco Previously Published Works

Title

Solid phase chemistry to covalently and reversibly capture thiolated RNA

Permalink

<https://escholarship.org/uc/item/2537s5k7>

Journal

Nucleic Acids Research, 46(14)

ISSN

0305-1048

Authors

Duffy, Erin E
Canzio, Daniele
Maniatis, Tom
[et al.](#)

Publication Date

2018-08-21

DOI

10.1093/nar/gky556

Copyright Information

This work is made available under the terms of a Creative Commons Attribution-NonCommercial License, available at <https://creativecommons.org/licenses/by-nc/4.0/>

Peer reviewed

Solid phase chemistry to covalently and reversibly capture thiolated RNA

Erin E. Duffy^{1,2}, Daniele Canzio³, Tom Maniatis³ and Matthew D. Simon^{1,2,*}

¹Department of Molecular Biophysics & Biochemistry, Yale University, New Haven, CT 06511, USA, ²Chemical Biology Institute, Yale University, West Haven, CT 06516, USA and ³Department of Biochemistry and Molecular Biophysics, Columbia University Medical Center, New York, NY 10032, USA

Received February 23, 2018; Revised June 04, 2018; Editorial Decision June 07, 2018; Accepted June 14, 2018

ABSTRACT

Here, we describe an approach to enrich newly transcribed RNAs from primary mouse neurons using 4-thiouridine (s⁴U) metabolic labeling and solid phase chemistry. This one-step enrichment procedure captures s⁴U-RNA by using highly efficient methane thio-sulfonate (MTS) chemistry in an immobilized format. Like solution-based methods, this solid-phase enrichment can distinguish mature RNAs (mRNA) with differential stability, and can be used to reveal transient RNAs such as enhancer RNAs (eRNAs) and primary microRNAs (pri-miRNAs) from short metabolic labeling. Most importantly, the efficiency of this solid-phase chemistry made possible the first large scale measurements of RNA polymerase II (RNAPII) elongation rates in mouse cortical neurons. Thus, our approach provides the means to study regulation of RNA metabolism in specific tissue contexts as a means to better understand gene expression *in vivo*.

INTRODUCTION

Tissue-specific regulation of steady-state RNA levels is achieved through the precise control of RNA synthesis, processing, and degradation. These dynamics are critical for control of global transcript levels. The rate of RNA synthesis is regulated through changes in RNA polymerase II (RNAPII) initiation and elongation in response to signaling (1). RNAPII elongation rates have been reported to vary >4-fold for a range of transcripts in mammalian cell culture (2–5), and these rates have been proposed to be determined by the regulation of co-transcriptional splicing, termination, and RNA stability (6). Factors including chromatin context (such as the presence of H3K79me2 in the gene body) are also shown to affect elongation rates (7,8). In addition, differences in the cell-type specific chromatin state, trans-acting factors, and cellular metabolism suggest that elongation rates may differ between tissues (9–11), but these rates have not been routinely studied in primary cells

or tissues. This is due to the fact that current experimental approaches have been limited by the scale required for biochemical enrichment (ca. 50 µg of input RNA is generally required for these protocols (12,13)). We therefore sought to develop more efficient biochemical capture of metabolically labeled RNA in order to understand RNA metabolism in primary cells using mouse cortical neurons.

Metabolic labeling allows the identification of newly synthesized RNAs by exposing cells to a non-canonical nucleoside that is incorporated during RNA synthesis. To identify newly synthesized RNA transcripts, total RNA is isolated and new, labeled RNAs are enriched. The three most widely used RNA metabolic labels are 5-bromouridine [BrU], 5-ethynyluridine [5-EU] and 4-thiouridine [s⁴U]. Depending on the nucleoside, labeled RNAs can be captured with a specific antibody (BrU) (14,15), or biotinylated using either click chemistry (5-EU) (16), or thiol-specific reactivity (s⁴U) (12,17,18), respectively (reviewed in 19). Enriched RNAs can be analyzed by RNA sequencing (RNA-seq), quantitative PCR (qPCR), or microarray. Protocols based on s⁴U are particularly useful because s⁴U allows both covalent and reversible capture and is rapidly incorporated into the cellular NTP pool in living cells without the need for cell lysis and nuclear isolation. In addition, s⁴U shows minimal perturbation to cellular physiology at low concentrations even after long treatment (17,18,20). Therefore, s⁴U metabolic labeling can be employed to study the stability of both rare, transient RNAs (21,22) as well as stable transcripts (20) in the same experiment (23).

Transcriptional elongation can be studied using 4sUDRB-seq, which combines transcriptional synchronization with s⁴U labeling (3). Specifically, cells are treated with 5,6-dichloro-1-β-D-ribofuranosylbenzimidazole (DRB), which blocks the release of paused RNAPII into productive elongation. After DRB is removed from the media, the wave of new transcriptional elongation can be followed by s⁴U metabolic labeling of the new RNAs (3). This approach has been used to calculate rates of transcription genome-wide in HeLa cells (3), but existing methods to capture new RNA require prohibitively large amounts input RNA material to study new transcription in mouse

*To whom correspondence should be addressed. Tel: +1 203 737 3274; Email: matthew.simon@yale.edu

cortical neurons. We therefore sought to use 4sUDRB-seq with an improved method to enrich s^4U -RNA in order to determine RNAPII elongation rates in mouse cortical neurons.

We recently published efficient chemistry for the enrichment of s^4U -RNA using the activated disulfide methane thiosulfonate (MTS), which improves yield and decreases biases in metabolic labeling experiments (18,24). We also identified two additional potential improvements that expand the scope of s^4U -RNA enrichment methods: decrease the number of steps in the protocol by directly conjugating the MTS activated disulfide to a solid support, and use higher stringency rinses in the context of a fully covalent system to decrease the amount of contaminating RNA without sacrificing yield. Here, we present a novel approach based on the synthesis of MTS-conjugated resin (MTS-resin) and confirmed that it could be used to distinguish fast- and slow-turnover RNAs in a metabolic labeling experiment. The MTS-resin also performed well in transient transcriptome sequencing (TT-seq) experiments where only very low levels of RNA are labeled with s^4U (22). Finally, we used this resin to measure RNAPII elongation rates in mouse cortical neurons using 4sUDRB-seq. These results reveal transcription elongation rates in primary neurons and highlight the diverse applications for small-scale s^4U -RNA purification in the study of RNA dynamics and metabolism.

MATERIALS AND METHODS

Cell lines and s^4U metabolic labeling

K562 cells were cultured in RPM1 media supplemented with 10% (v/v) fetal bovine serum, and 1% (v/v) penicillin/streptomycin. HEK293T cells were cultured in high glucose DMEM media supplemented with 10% (v/v) fetal bovine serum, and 1% (v/v) 2 mM L-glutamine. Cultured cells were treated with s^4U as described below and harvested at 80% confluence by the addition of 1 ml TRIzol. For TT-seq, K562 cells were treated with 1 mM s^4U for 5 min. For s^4U Chase-seq experiments, K562 cells were treated with 1 mM s^4U for 2 h. s^4U -containing media was exchanged with RPM1 media containing 20 mM uridine, and cells were harvested after 0.5 or 18 h of incubation. HEK293T cells were treated with 100 μ M s^4U for 2 h. Cells in TRIzol were flash frozen and stored overnight at -80°C .

Mouse cortical neurons and 4sUDRB

Mouse cortical neurons were isolated at E18 as previously described (25). About 2×10^6 cells were plated per six-well dish. Two days post isolation, cells were treated with DRB for 3 h or with DMSO for the minus DRB control. 4sUDRB experiments were performed as previously described (26) with the following changes: (i) Cells were treated with 1 mM s^4U for 30 min before being collected; (ii) cells were collected 0, 10, or 20 min after DRB removal. Cells were harvested with TRIzol, flash frozen and stored at -80°C .

Purification of total RNA

Cell lysates were chloroform extracted once and precipitated with one volume of isopropanol (supplemented with

100 μ M DTT and 5–10 μ g glycobule), incubated for 10 min at room temperature and centrifuged at $20\,000 \times g$ for 20 min at 4°C . The pellet was washed with an equal volume of 75% ethanol. Purified RNA was dissolved in RNase-free water to a concentration of 200 ng/ μ l. Contaminating DNA was digested with Turbo DNase (1 U per 10 μ g RNA, 37°C , 30 min.) Samples were purified by phenol:chloroform extraction followed by a second isopropanol precipitation and resuspension in 40 μ l of RNase-free water. For sheared RNA samples, $2\times$ fragmentation buffer (40 μ l, 150 mM Tris pH 8.3, 225 mM KCl, 9 mM MgCl_2) was added to the RNA and incubated at 94°C for 4 min. Samples were immediately placed on ice and quenched with EDTA (20 μ l 250 mM EDTA, final concentration 50 mM). Samples were cooled on ice (2 min) and were purified by the following modification of the RNeasy MinElute Cleanup Kit (Qiagen). 350 μ l of buffer RLT and 250 μ l of 100% EtOH were added to the RNA sample and placed over an RNeasy column. Columns were centrifuged for 15 s at $12\,000 \times g$, 4°C , and flow through was discarded. Columns were washed with 500 μ l buffer RPE supplemented with 35 μ l of 1% β -me (final concentration 10 mM β -me) and centrifuged as above. Columns were washed with freshly prepared 80% EtOH and centrifuged for 2 min at $12\,000 \times g$, 4°C , and flow through was discarded. Columns were dried by centrifugation at maximum speed for 5 min at 4°C . Samples were eluted into a fresh microfuge tube with 14 μ l RNase-free water and centrifuged at maximum speed for 1 min at 4°C .

Synthesis of MTS-resin

For 10 samples, 100 μ l NHS magnetic sepharose (GE Healthcare) was added to 1 ml RNase-free water, mixed well, and captured on a magnetic rack, discarding supernatant. One milliliter ice cold 1 mM HCl was added to beads, incubated 2 min with agitation, and beads were captured on a magnetic rack, discarding supernatant. Beads were washed twice with 1 ml $1\times$ PBS, then 100 μ l MTSEA (Biotium, 10 mg/ml in PBS) plus 0.75 μ l DIEA was added. Beads were incubated at room temperature for 15 min with rotation. Beads were washed twice with 1 ml $1\times$ PBS and blocked with 1 ml blocking buffer ($1\times$ PBS, 5 μ l acetic anhydride) for 15 min with rotation. Beads were washed twice with 1 ml $1\times$ PBS and twice with 1 ml quench buffer (1 M Tris pH 7.4, 200 mM ethanolamine). Beads were quenched with 1 ml quench buffer for 15 min with rotation. Beads were washed twice with 1 ml quench buffer and twice with 1 ml binding buffer (100 mM NaCl, 10 mM HEPES pH 7.4, 1 mM EDTA, 0.05% Tween). Beads can be stored at 4°C for several hours in binding buffer or aliquoted (10 μ l/sample) and binding buffer removed to use immediately.

Purification of s^4U -RNA with MTS-resin

1–5 μ g total RNA in 10.5 μ l RNase-free water was mixed with 1.5 μ l $10\times$ binding buffer (1 M NaCl, 100 mM HEPES pH 7.4, 10 mM EDTA, 0.5% Tween), and 3 μ l DMF, added to MTS-resin (10 μ l aliquot), and incubated at room temperature in the dark for 2 h with rotation. Beads were captured on a magnetic rack and supernatant removed. Beads were incubated for 5 min with the following wash buffers:

once with 100 μ l 1 \times binding buffer, twice with 100 μ l high salt wash buffer (1 M NaCl, 100 mM Tris pH 7.4, 10 mM EDTA, 0.05% Tween), twice with 100 μ l denaturing buffer (8 M guanidinium chloride) and three times with 100 μ l buffer TE (10 mM Tris pH 7.4, 1 mM EDTA) at 55°C. RNA was eluted with 10 μ l elution buffer (100 mM NaCl, 10 mM Tris pH 7.4, 1 mM EDTA, 10 mM DTT and 100 pg fragmented total RNA from *S. pombe* (a generous gift from the Berro lab, Yale University) and incubated at room temperature in the dark for 15 min with rotation. Eluent was ethanol precipitated with 5–10 μ g glycoblue, and RNA concentration was assayed by Bioanalyzer RNA 6000 Pico Kit (Agilent) according to the manufacturer's instructions.

MTS-resin binding capacity

A solution of 100 nmol s^4 U nucleoside in 18 μ l RNase-free water was mixed with 3 μ l 10 \times binding buffer and 6 μ l DMF (total volume 30 μ l) was enriched using 1, 2, 5, 10 or 20 μ l MTS-resin as above. Enriched nucleoside was quantified by UV-vis spectroscopy based on A_{334} absorbance, and resin binding capacity was calculated using a standard curve of different concentrations of s^4 U.

MTS-resin saturation

1 μ g of total RNA from K562 cells (prepared as above) was combined with 1 ng total RNA from *S. pombe* and enriched on 1, 2, 5, 10, 20 or 40 μ l MTS-resin as above. Enriched RNA and 10% input were each reverse transcribed using the Superscript VILO cDNA synthesis kit (Invitrogen) and analyzed by qPCR using iTaq Universal SYBR Green Supermix (Bio-Rad). Enrichment of s^4 U-RNA was analyzed using *H. sapiens* qPCR primers for CDKN1B total RNA (Forward: 5'-TTTGACTTGCATGAAGAGAAGC-3' and Reverse: 5'-AGCTGTCTCTGAAAGGGACATT-3') (27). Background from *S. pombe* RNA was analyzed using *S. pombe* qPCR primers for 28S rRNA (Forward: 5'-TGAGAAGGGATGTTGGACCTGCTT-3' and Reverse: 5'-ATTGCGTCAACACCACTTTCTGGC-3') (28).

Comparison between MTS biotin and MTS-resin enrichment

1 μ g of total RNA from HEK293T cells was combined with 1 ng total RNA from *S. pombe* and enriched with MTS biotin exactly as in (29) or with MTS-resin as above. Enriched samples were assayed by RT-qPCR as above and fold enrichment was calculated as

$$\frac{2^{(C_i(\text{Enriched}_{Hs}) - C_i(\text{Input}_{Hs}))}}{2^{(C_i(\text{Enriched}_{Sp}) - C_i(\text{Input}_{Sp}))}}$$

An RNA ladder of 100–1000 nt was transcribed *in vitro* using the RNA Century Plus Marker Template and Maxiscript T7 transcription kit (Invitrogen) using Cy5-CTP at a ratio of 1:1 Cy5-CTP:CTP for downstream visualization, with the option of adding s^4 UTP (TriLink Biotechnologies) at a ratio of 1:1 s^4 UTP:UTP to the reaction. After the reaction, template DNA was digested with Turbo DNase (Thermo Fisher). Enzymes were removed by phenol-chloroform extraction and the RNA was purified using the RNeasy Mini Kit (QIAGEN) with the following

changes: β -mercaptoethanol was added to wash buffer RPE to a final concentration of 1%. 400 ng of RNA ladder was enriched with MTS-resin following the protocol described above, or with HPDP-biotin and MTS-biotin following protocols in (18). Enriched samples were separated on a 5% urea-PAGE gel, visualized by Typhoon fluorescence imager (GE), and bands were quantified using ImageJ software.

Library preparation and sequencing

10 ng input as well as enriched RNA were prepared using the SMARTer Stranded Total RNA-seq Pico Input Mammalian Kit (Clontech) according to the manufacturer's instructions. Samples were multiplexed with Illumina TruSeq i7 barcodes, and sequencing was performed at the Yale Center for Genomic Analysis on Illumina HiSeq 2500 instruments with paired-end 2 \times 75 nt sequencing runs.

Bioinformatic analysis

Sequencing reads were aligned using STAR (version 2.4.2a) (30) to a joint index of the *H. sapiens* and *S. pombe* genomes (GRCh38 and sp2) and transcriptomes (NCBI and Ensembl Fungi v22; respective) or to the *M. musculus* genome and transcriptome (GRCm38, NCBI) (31,32). Alignments and analysis were performed on the Yale High Performance Computing clusters. Following alignment, HTSeq-count (version 0.6.1p1) (33) was used to quantify annotated *H. sapiens* and *S. pombe* transcripts for total RNA (-t gene) and mRNA (-t exon). Tracks normalized using the *S. pombe* reads were uploaded to the UCSC genome browser. Pearson correlations between samples were visualized in R using the corrplot package. GO-enrichment analysis was performed using the PANTHER classification system (34) using the statistical overrepresentation test and GO molecular function—complete gene list. TT-seq data from Schwalb *et al.* (GEO series accession GSE75792) were randomly downsampled for the same read depth as MTS-TT-seq data and processed as above. Counts were filtered to remove mitochondrial and ribosomal RNAs. PRO-seq data were downloaded from GEO (series accession GSM1480327), and ChIP data for RNAPII, H3K36me3 and H3K4me1 were downloaded from the ENCODE ChIP data matrix. Enhancer RNAs were quantified using BEDtools coverage (50% minimum read overlap) of the Chromatin State Segmentation by HMM from ENCODE/Broad (35) and filtered for strong enhancers. MicroRNA transcription start sites were assigned using the mirSTP pipeline (36) and relaxed annotations are reported.

RNAPII elongation rates were calculated using the scripts published by Fuchs *et al.* (3), with the following modifications: (i) Due to the lower sequencing depth in our samples, the bin size was changed from 100 to 500 bp. (ii) Because the time of s^4 U metabolic labeling was 10 and 20 min, rather than 4 and 8 min published by Fuchs *et al.*, we expanded our x-intercept filtering to -2.5 min to 10 min, rather than -1 to 4 min. (iii) We calculated rates for the most abundant isoform of each transcript. To expand our analysis to more genes, we also calculated RNAPII elongation rates from 0 to 10 min, assuming a linear fit (e.g. a constant rate of transcription). Genes were filtered for expression (RPK > 1), active RNAPII elongation over 20 min

following DRB washout (average transcriptional boundary at 20 min is greater than the average transcriptional boundary at 10 min), agreement of two replicates (transcriptional boundary of replicate 1 within 70% of replicate 2). In addition, we only considered genes where the transcriptional boundary of one transcript did not overlap another gene.

H3K79me2 and H3K36me3 ChIP data from mouse cortical neurons (GEO series accession GSE95831 and GSE103214 (37), respectively) were re-processed as follows: reads were aligned to the mm10 genome using Bowtie2 (38) and \log_2 fold enrichment over input was calculated using MACS2 (39). Mean fold enrichment was calculated over the first 10 kb from the TSS.

RESULTS

Resin synthesis and characterization

Developing solid-phase chemistry to capture s^4U -RNA requires the use of a highly activated disulfide, as the loading of the resin limits the extent to which mass-action can be used to drive the chemical reaction. Previously, we demonstrated that methane thiosulfonate (MTS) activated disulfides react more efficiently with s^4U than the commonly used HPDP-biotin, and that this improved chemistry enables more sensitive applications of s^4U metabolic labeling (18). We hypothesized that coupling the MTS moiety directly to magnetic sepharose beads should decrease the loss that occurs during the multiple steps of a biotin/streptavidin purification and increase fold enrichment of s^4U -RNA by enabling higher stringency rinses. After s^4U -RNAs are eluted by reducing the disulfide bond, these RNAs could be analyzed by microarray, qPCR, or RNA-seq. To test this approach, we coupled methane thiosulfonate (MTS) to a solid support (Figure 1) by reacting methane thiosulfonate ethylamine (MTSEA) with commercially available N-hydroxysuccinimide (NHS) activated magnetic beads using a modification of standard protocols (Supplementary Figure S1A, Materials and Methods). We found these beads are capable of capturing s^4U nucleosides as well as metabolically labeled s^4U -RNA (Figure 1B and C).

To determine the binding capacity of MTS-resin, we incubated beads with a vast molar excess of s^4U nucleoside to saturate the available sites on the resin. After rinsing and elution, we quantified the amount of the captured nucleoside. Binding was linear with increasing quantity of resin and the resin could capture 0.4 nmol s^4U per μL MTS-resin slurry (Figure 1C). While this loading capacity provides an upper bound of the amount of s^4U -RNA that can be captured, other factors such as site accessibility could provide practical limits to the resin loading in a biological sample. Therefore, we used metabolically labeled RNA from K562 cells (2 h, 1 mM s^4U) to test the relationship between amounts of MTS-resin slurry used and the amount of s^4U -RNA retrieved (Figure 1D). We observed an increase in s^4U -RNA enrichment with increasing amounts of MTS-resin (plateauing at 10 μL resin per μg of input RNA). To measure nonspecific background, we also added exogenous unlabeled RNA from *S. pombe* (1 ng unlabeled standard per 1 μg input labeled RNA) and found that this background did not significantly increase even at the highest

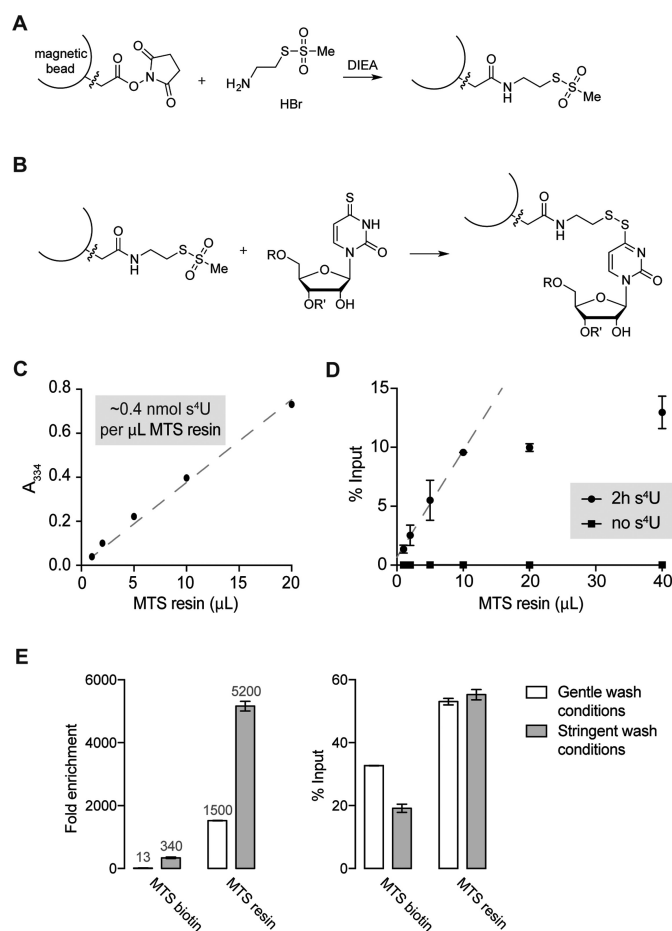


Figure 1. MTS-resin covalently and reversibly enriches s^4U -RNA. (A) Scheme of MTS-resin synthesis. (B) Scheme of MTS-resin reactivity with s^4U . (C) Quantification of MTS-resin loading capacity with free s^4U nucleoside. Molar excess of s^4U was enriched with increasing volumes of MTS-resin, and eluted nucleoside concentration was measured by A_{334} absorbance. Binding capacity was calculated by linear regression of absorbance and converted to nmol s^4U based on a standard curve. (D) Quantification of MTS-resin loading capacity for total RNA. Total RNA from K562 cells was metabolically labeled with 1 mM s^4U for 2 h, spiked with non-labeled RNA from *S. pombe* as an internal non- s^4U control, and reacted with increasing volumes of MTS-resin. Enriched RNA was quantified by RT-qPCR using primers for *H. sapiens* (2 h s^4U) and *S. pombe* (no s^4U) transcripts. Percent input was quantified relative to a 10% input RNA sample. (E) Comparing enrichment by MTS biotin and MTS-resin methods. Metabolically labeled total RNA from HEK293T cells was spiked with non-labeled RNA from *S. pombe* as an internal non- s^4U control and enriched using MTS biotin (29) or MTS-resin using gentle or stringent wash conditions (described in Materials and Methods). Fold enrichment (left panel) was calculated as s^4U -RNA transcript enriched from the human sample ($\%Input_{HS}$) divided by signal from the background sample ($\%Input_{SP}$). Percent input (right panel) was calculated as in (D). Error bars in D and E represent SD of two technical replicates.

amounts of MTS-resin that we tested. While background did not increase, we did observe some bias for enrichment of longer RNAs (with more s^4U) when using the MTS-resin that is not observed with MTS-biotin (Supplementary Figure S1B–D). This type of length bias has been observed previously (40) and can be mitigated by pre-shearing RNA samples before enrichment (22).

Next, we compared the sensitivity of this small-scale s^4U -RNA enrichment (1 μg input RNA) on MTS-resin to our previously published protocols using MTS-biotin (18,29) and tested the effect of stringent rinses on both purifications (Figure 1E). We measured the retrieval of a metabolically labeled mRNA (*CDKN1B*) in comparison with an unlabeled RNA from *S. pombe*. While stringent rinses improve the fold enrichment in MTS biotin experiments (13-fold enrichment with standard rinses, 340-fold with stringent rinses), the enrichment was significantly increased with MTS-resin (1500-fold enrichment with standard rinses, 5200-fold with stringent rinses). In addition, while the stringent rinses decrease s^4U -RNA yield in MTS biotin purification (33% input with standard rinses, 19% input with stringent rinses), we did not detect a significant difference in yield with MTS-resin enrichment stringent rinses (53% input with standard rinses, 55% input with stringent rinses). These results demonstrate that high levels of enrichment can be achieved when using an entirely covalent purification, which was made possible by the MTS-resin.

4-Thiouridine pulse-chase labeling (s^4U Chase-seq)

After we synthesized MTS-resin and validated that it can capture s^4U -RNA, we next tested if the MTS-resin could be used to distinguish fast turnover RNA populations from slower turnover populations, a common application of s^4U metabolic labeling experiments (12,17,40,41). We chose to perform a pulse-chase experiment similar to Yi *et al.* (20), where the cells are exposed to a s^4U pulse (1 mM, 2 h) followed by a chase phase where the cells were treated with 20 mM uridine (Figure 2A). Those RNAs that were labeled with s^4U at 0.5 h were compared with the population of s^4U -RNA that remained after 18 h to detect long-lived RNAs. We chose a short 2 h pulse that leads to only small amounts of s^4U -RNA, but provides a stringent test of the resin. To optimize this s^4U -chase labeling, longer treatments could be used, as s^4U can be present in cells for several days without affecting RNA dynamics due to its low toxicity (17,18,20). To ensure that this experiment could be performed on a scale compatible with cells from primary tissues, we used only RNA from $\sim 2 \times 10^6$ cells for the enrichment. This low quantity of input RNA (1 μg of total RNA) contrasts with the higher quantities (generally $> 25 \mu\text{g}$) used in previous pulse-chase experiments using s^4U (20,42,43).

We used high-throughput sequencing to analyze s^4U -RNA from both the 0.5 h and 18 h chase that had been enriched with MTS-resin. Counts of the aligned reads revealed consistent enrichment across biological replicates (triplicate, Pearson's $r = 0.87$ – 0.97 , Supplementary Figure S2A). The relative stability of each transcript could be inferred based on the relative levels of different RNAs in the 0.5 h versus 18 h s^4U populations (Figure 2B and C). We expect fast-turnover mRNAs to be under-represented relative to the population in the 18 h chase and slow-turnover mRNAs to be over-represented. Previously identified fast- and slow-turnover transcripts (44,45) showed expected s^4U profiles in genome browser tracks (Figure 2B, Supplementary Figure S2C). To determine which RNAs displayed relatively fast or slow turnover compared to the entire transcriptome, we performed differential expression analysis on the s^4U -RNAs

enriched after a short chase (0.5 h) versus a long chase (18 h) with uridine (Figure 2C). Using standard differential expression analysis pipelines (DESeq2, $P_{\text{adj}} < 0.05$), we identified over a thousand RNAs that were enriched in each category (1757 RNAs as fast turnover; 1571 RNAs as slow turnover). A full list of fast and slow turnover transcripts can be found in Supplementary Table S1. Because mRNA stability has been tied to protein function (44,45), we analyzed the transcripts by GO-enrichment analysis (Supplementary Figure S2D) and found that the results were consistent with previous data. For example, transcripts encoding transcription factors and histone mRNAs are enriched within fast turnover RNAs (44,46), whereas mRNAs for proteins involved in biosynthetic processes were enriched within slow turnover RNAs (44,45). In addition, the \log_2 fold difference between s^4U -RNA in the 0.5 h and 18 h chase correlates with genome-wide RNA half-lives calculated by Schofield *et al.* (Pearson's $r = 0.58$, Figure 2D) and Friedel *et al.* (Pearson's $r = 0.63$, Supplementary Figure S2C) (45,47). Slow-turnover transcripts had a significantly longer half-life on average compared to transcripts that were not identified as significantly fast- or slow-turnover ($P < 2.2 \times 10^{-16}$); conversely, fast-turnover transcripts had a significantly shorter half-life on average ($P < 2.2 \times 10^{-16}$; Figure 2E). These results demonstrate that MTS-resin can be used to purify s^4U -RNA from small numbers of cells and can distinguish fast and slow turnover transcripts.

MTS-resin-based transient transcriptome sequencing (MTS-TT-seq)

For applications such as measuring transcription elongation rates in primary cells, a s^4U -RNA capture method must perform well at small scale and also have the sensitivity to capture rare, newly made RNAs from the higher concentrations of pre-existing RNA pool. We tested MTS-resin in the context of a transient transcriptome sequencing (TT-seq) experiment (Figure 3A), which uses very short s^4U labeling (5 min, 1 mM) followed by RNA fragmentation and enrichment. This approach captures rare RNAs including introns, enhancer RNAs (eRNAs), and pri-miRNAs (22). Using MTS-resin, we performed this experiment using only 2.5 μg of input RNA, substantially below (>20 -fold) the scale that is generally used for these experiments (22,48). Enriched RNA samples, as well as input RNA, were analyzed by high-throughput sequencing and reads were mapped to the human genome. Enrichment was consistent across biological replicates (Pearson's $r = 0.99$). As we would expect if the MTS-resin successfully enriched the transient RNA population, the MTS-TT-seq samples correlate better with each other than with $-s^4U$ controls or input, suggesting that the resin is capturing new transcripts over nonspecific background (Figure 3B, Supplementary Figure S3B). Consistent with this conclusion, MTS-TT-seq samples correlated well with previously published TT-seq data (Pearson's $r = 0.89$, Supplementary Figure S3A and B). Notably, we found that MTS-TT-seq enriches transient RNA species including pre-mRNA (as revealed by intronic RNA enrichment), eRNAs, and primary microRNAs (pri-miRNAs) relative to input (Figure 3C and D), consistent with previous data (22). We conclude that MTS-resin is able to enrich rare RNA pop-

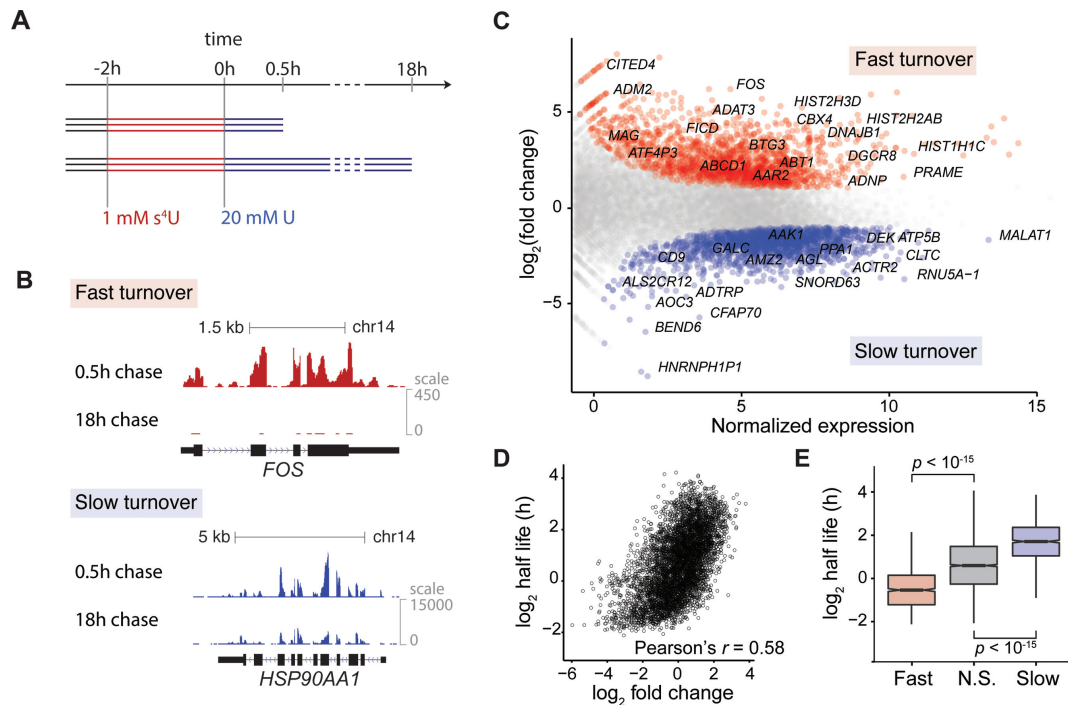


Figure 2. s⁴U Chase-seq identifies fast- and slow-turnover RNAs in K562 cells. (A) Schematic of s⁴U Chase-seq. K562 cells were metabolically labeled with 1 mM s⁴U for 2 h, followed by a 20 mM uridine chase for 0.5 h or 18 h. (B) Example genome browser view of s⁴U-RNA enriched after 0.5 h and 18 h uridine chase. *FOS* and *HSP90AA1* were identified as fast and slow turnover, respectively, by differential expression analysis. Reads from biological triplicates were summed for display. (C) Scatterplot of fold change versus normalized expression based on comparative analysis of RNAs that are significantly enriched or depleted in early time points (0.5 h chase) relative to late time points (18 h chase). Fast-turnover RNAs (fold difference > 2; $P < 2 \times 10^{-5}$) are colored red; slow-turnover RNAs (fold difference < 0.5; $P < 2 \times 10^{-5}$) are shown in blue. (D) Scatterplot of log₂ fold change from (C) versus log₂ RNA half-life from Schofield *et al.* (E) Box and whisker plot of log₂ RNA half-life from Schofield *et al.* for RNAs binned as fast turnover, slow turnover, or not significant in (C). RNAs were filtered for normalized expression > 2 (logCPM).

ulations from small numbers of cells with similar efficiency to existing methods at higher scale.

Unlike other methods to analyze transient RNA species such as GRO-seq and PRO-seq (14,49), s⁴U-based methods do not require purification of nuclei. However, despite the biochemical challenge of these protocols, GRO-seq and PRO-seq have been more extensively validated than analogous s⁴U enrichment techniques. Therefore, we wondered whether data from MTS-TT-seq could be analyzed using analysis pipelines originally developed for these validated approaches. To test this, we attempted to identify the active transcription start sites of intergenic miRNAs using a recently developed bioinformatics pipeline for GRO-seq and PRO-seq data called mirSTP (36). mirSTP uses divergent sharp peaks around transcription start sites and continuous coverage over active transcription regions to identify intergenic miRNA TSSs. Analyzing our MTS-TT-seq data with this pipeline, we were able to identify 89 TSSs in K562 cells (Figure 3D, complete list of miRNA TSSs in Supplementary Table S2). Of the 89 TSSs discovered by TT-seq, 50 overlapped with the 90 TSSs annotated by mirSTP using GRO-seq data, which is consistent with the proportion of overlap observed between mirSTP and Hua *et al.*, which identifies miRNA TSSs using H3K4me3 and DNase I hypersensitive sites (36,50). These data demonstrate that GRO-seq bioinformatics pipelines can be successfully used to analyze MTS-TT-seq data. In addition, the smaller scale

afforded by MTS-resin for TT-seq analysis led us to conclude that this approach will allow the study of transcriptional dynamics analyses in a wider variety of cell types and tissues than was previously feasible.

RNAPII elongation rates in mouse cortical neurons

Having established that MTS-resin is compatible with s⁴U-RNA capture from small numbers of cells, we next applied the resin in the context of a 4sUDRB-seq experiment to study the transcriptional dynamics in primary neurons. We treated $\sim 2 \times 10^6$ neurons with DRB to synchronize RNAPII at the promoter-proximal pause site. Next, s⁴U was added to the media (before DRB washout to allow s⁴UTP to build up in the cellular pool) and the DRB was removed to allow the polymerase to elongate and incorporate s⁴U into the newly synthesized RNA. Total RNA from cells harvested after 0, 10 or 20 min of DRB washout was purified, and s⁴U-RNA was enriched on MTS-resin followed by high-throughput sequencing (Figure 4A and Supplementary Figure S4A).

Read counts mapping to transcripts were consistent between biological replicates (Pearson's $r = 0.81$ – 0.97). As we would expect if 4sUDRB-seq is capturing the transcriptional wave of newly synthesized RNA, $t = 10$ min samples correlated better to $t = 20$ min (Pearson's $r = 0.81$ – 0.90) than to RNA-seq (Pearson's $r = 0.58$ – 0.63), $t = 0$ min (Pearson's $r = 0.58$ – 0.67) or no treatment controls (Pearson's $r =$

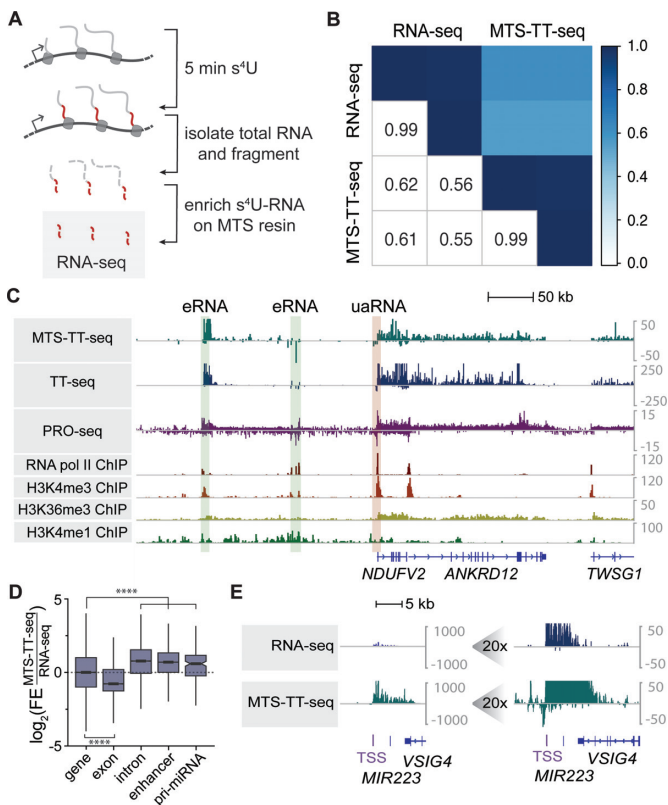


Figure 3. MTS-TT-seq captures unstable RNAs. (A) Scheme of TT-seq enrichment using MTS-resin. K562 cells were metabolically labeled with 1 mM s^4U for 5 min, followed by total RNA isolation and fragmentation to ~ 200 nt. RNA fragments containing s^4U are enriched on MTS-resin and analyzed by RNA-seq (B) Heatmap of pairwise correlation coefficients between MTS-TT-seq (Pearson's $r = 0.99$) and RNA-seq (Pearson's $r = 0.99$) biological replicates. (C) Box plot of \log_2 fold enrichment of unstable RNA populations in MTS-TT-seq compared to RNA-seq. **** $P < 0.0001$. Pseudo-count of 1 was added to all input counts. (D) Example genome browser view showing enrichment of transient species such as introns, antisense transcription (orange box) and enhancer RNAs (green boxes) [chr18:8,836,895-9,370,470] in MTS-TT-seq, TT-seq (22), and GRO-seq (49), as well as ChIP data from RNAPII, H3K4me3, H3K36me3 and H3K4me1 histone marks (55). Reads above the x -axis indicate transcription on the forward strand, whereas reads below the x -axis indicate transcription on the reverse strand. (E) Example transcription start site (TSS) of MIR223 identified using MTS-TT-seq and the mirSTP pipeline. The left panel shows normalized signal in RNA-seq and MTS-TT-seq data, while the right panel (zoomed in y -axis) shows bidirectional transcription at the TSS in MTS-TT-seq.

0.67–0.72 Supplementary Figure S4B). In addition, the $t = 10$ min, $t = 20$ min, and no treatment samples contained a higher proportion of reads mapping to introns compared to the $t = 0$ min samples, consistent with the expectation that 4sUDRB-seq enriches for nascent RNA (Supplementary Figure S4C).

We observed a transcriptional wave in the $t = 10$ min and $t = 20$ min samples in which the nascent RNA reads in the $t = 20$ min sample extended much beyond the $t = 10$ min sample relative to the TSS (Figure 4B and C). These profiles are similar to those demonstrated in HeLa cells (3), despite using 20-fold less RNA for enrichment (Figure 4B and C). We sought to calculate the mean elongation rate of RNAPII during the first 10 min and first 20 min of DRB washout.

After filtering the RNAPII transcriptional boundary for RNA-seq expression and agreement between replicates (see Materials and Methods), the RNAPII elongation rate from 0 to 10 min after DRB washout was calculated to be much faster than the elongation rate from 10 to 20 min for most genes (Supplementary Figure S4E), which is consistent with previous reports that RNAPII reaches its maximum elongation speed approximately 15 kb through the gene (51). Therefore, we first calculated the elongation rate from 0 to 10 min following DRB washout, which is a timescale more consistent with previous experiments in cell culture (3,8). We estimated the rates of RNAPII elongation from 0 to 10 min after DRB washout for 260 genes in mouse cortical neurons, where the median transcription elongation rate was 2.74 kb/min, and gene-specific elongation rates varied from 0.35 to 5.83 kb/min (Figure 4D, Supplementary Table S3).

We examined how the gene-specific rates of RNAPII elongation in mouse cortical neurons related to the presence of chromatin modifications that have been previously reported to correlate with RNAPII elongation rate in cell culture (3,8,51). We found H3K79me2 to be significantly enriched in the fastest quartile (Wilcoxon test, $P = .0024$), whereas H3K36me3 did not show any significant enrichment ($P = .22$, Figure 4E). We did not find any significant correlation between RNAPII elongation rate and gene length, expression, or exon density (Figure 4E).

In an effort to quantify RNAPII elongation rates using transcriptional boundaries calculated after 10 and 20 min of DRB washout, we more stringently filtered our transcriptional boundary measurements using criteria established by Fuchs *et al.* (26). We limited our analysis to the most abundant isoform of transcripts > 50 kb in length where transcriptional boundary algorithms (see Materials and Methods) gave convergent values for both biological replicates in the $t = 10$ and $t = 20$ min samples. In addition, we filtered our elongation rates for an x -intercept between -2.5 min and 10 min, which is proportional to the longer times used in our experiments (10 and 20 min, compared to 4 and 8 min in (3)). Based on these conservative criteria, we were able to calculate the elongation rate for 55 genes in cortical neurons (Figure 4F, G, Supplementary Table S4). The s^4U -RNAs that mapped to these regions show a similar transcriptional wave compared to the profile for all genes > 50 kb (compare Supplementary Figure S4D and Figure 4C). We found that the median transcription elongation rate in mouse cortical neurons for these transcripts was 2.95 kb/min, which is similar to the median transcription elongation rate that Fuchs *et al.* calculated in HeLa cells (3.72 kb/min) (3). In addition, the RNAPII elongation rate varied more than 3-fold between genes (1.5 to > 6 kb/min), which is consistent with the spread of RNAPII elongation rates from 0 to 10 min (Figure 4D), as well as previous findings in cell culture (2–5).

DISCUSSION

Here we show that MTS conjugated to beads can be used to capture s^4U metabolically labeled RNA. This one-step enrichment reduces handling loss that is inherent in other s^4U enrichment protocols, and thereby makes it possible to use

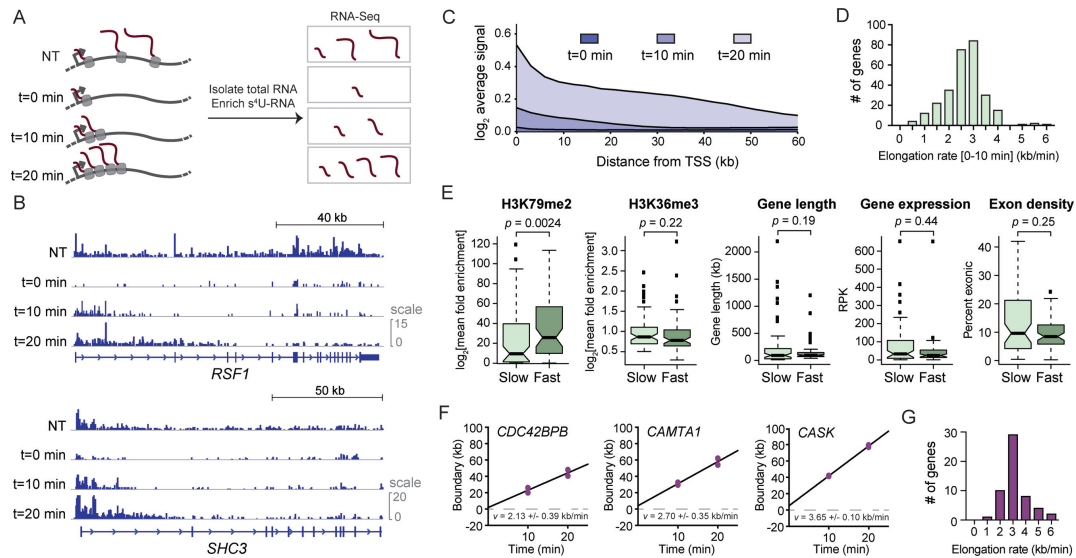


Figure 4. MTS-resin reveals RNAPII elongation rates in mouse cortical neurons. (A) Scheme of 4sUDRB-seq using MTS-resin. NT: no DRB treatment (30 min s^4U -seq); $t = 0$ min: no DRB washout. s^4U is added to cells for 30 min, but DRB is not removed from cells; $t = 10$ min, $t = 20$ min: s^4U -RNA enrichment after 10 or 20 min DRB washout. Total RNA is purified from cells and s^4U -RNA is enriched with MTS-resin, followed by high-throughput sequencing. (B) 4sUDRB-seq enriched RNA from two representative genes, *Rsf1* and *Shc3*. Arrows mark the direction of transcription. (C) Average distribution of reads in all genes longer than 50 kb from s^4U -RNA enriched after 0, 10 or 20 min of DRB removal from two biological replicates. (D) Distribution of RNAPII elongation rates from 0 to 10 min following DRB washout, calculated from 260 genes in cortical neurons. (E) Box-whisker plot of \log_2 transformed H3K79me2 and H3K36me3 mean fold enrichment in the first 10 kb from the TSS, gene length (kb), gene expression (RPK), and exon density (% exon) of the 25% of genes with the highest calculated elongation rate and the 25% of genes with the lowest elongation rate. P -values were calculated by the Wilcoxon test. (F) Linear fit of transcriptional boundaries calculated after 10 and 20 min of DRB washout. The slope (v) represents the elongation rate in kb/min, with confidence intervals as indicated. (G) Distribution of RNAPII elongation rates calculated from 55 genes in cortical neurons using criteria established by Fuchs *et al.* (3).

20–50-fold less input RNA. We demonstrate that this resin can capture s^4U -RNA from small numbers of cells, and we identify fast- and slow-turnover transcripts in K562 cells using s^4U Chase-seq. These results correlate well with published RNA half-lives (45,47). In addition, we use MTS-resin to capture transient RNA species including introns, eRNAs, and pri-miRNAs in K562 cells in the context of a TT-seq experiment, but with much less input material. We demonstrate that these data correlate well with published data where higher amounts of RNA were used. In addition, the bioinformatic pipeline mirSTP, as well as other pipelines originally developed for GRO-seq and PRO-seq data, can be applied to MTS-TT-seq in order to identify intergenic miRNA TSSs.

Using MTS-resin, we were able, for the first time, to measure RNAPII elongation rates in cortical neurons. We first estimated the rate of RNAPII elongation during the first 10 min following DRB washout and found gene-specific differences in rates. These differences are likely to be important for co-transcriptional processes like alternative splicing and RNA degradation (52). To this end, we sought to identify chromatin marks and gene features that correlate with RNAPII elongation. Our data show a positive correlation between elongation rate and H3K79me2, a finding that has been previously observed in cell culture (3,8,51). The H3K79 methyltransferase Dot1 can be recruited to RNAPII during transcription (53), but the mechanism by which H3K79me2 influences the rate of RNAPII elongation remains unknown.

In addition, we sought to analyze RNAPII transcription boundaries after both 10 and 20 min of DRB washout using the more stringent criteria established by Fuchs *et al.* (3) which focuses on rates that are linear during this time-course. This limited set of 55 genes showed a similar median elongation rate to the larger set of RNAPII elongation rates during the first 10 min of DRB washout (2.74 versus 2.95 kb/min). Despite the differences in metabolic state of primary neurons compared to rapidly dividing HeLa cells, the median transcription rates are remarkably similar (3 kb/min in neurons versus 3.7 kb/min, Figure 4D). We found that these rates vary >3-fold across the set of genes we analyzed, which is consistent with rates reported in cell culture (2–5). Given the extensive differential processing of RNA in neurons in particular (54), the ability to measure RNAPII elongation rates in mouse cortical neurons provides the foundation for understanding the relationship between the control of RNA elongation and the generation of different neuronal RNA isoforms.

These results demonstrate how MTS-resin can be a useful tool for studying RNA population dynamics in samples where input RNA is limiting. We suggest that MTS-resin is particularly well suited for smaller-scale purification of s^4U -RNA (e.g. primary tissues or microdissections). When large quantities of RNA are available, MTS-biotin has some advantages over MTS-resin. When using MTS-biotin, higher concentrations of the activated disulfide can be used to drive s^4U -RNA modification, but an additional step is required to remove unreacted MTS-biotin. When using MTS-resin, we have observed variable amounts of length bias

(bias toward enrichment of transcripts with more uridine nucleotides, Supplementary Figure S1B–D) which is not observed with MTS-biotin (18). On the other hand, as we have demonstrated here, MTS-resin reduces handling and increases the stringency of purification through a fully covalent capture. Furthermore, concerns about length bias during enrichment can be addressed by shearing the RNA prior to enrichment as was established for TT-seq (22), a step that was included in all the experiments presented here. Therefore, MTS-resin expands the existing metabolic labeling toolkit to simultaneously study transient and stable RNAs in the same experimental setup, thereby providing a glimpse into the complex transcriptional network of a variety of cell types such as primary neuronal cultures.

DATA AVAILABILITY

Raw and processed RNA-seq datasets have been submitted to the NCBI Gene Expression Omnibus under the accession code GSE110951.

SUPPLEMENTARY DATA

Supplementary Data are available at NAR Online.

ACKNOWLEDGEMENTS

We thank members of the Simon lab for helpful discussions and comments on the manuscript, Eliot Coffey, Chiamaka Nwakeze and Sandy Rajkumar from the Maniatis lab for help with the dissection of cortical neurons and for helpful discussions on the manuscript.

FUNDING

National Science Foundation [DGE1122492 to E.E.D.]; National Institute of Health [T32GM007223 to E.E.D., R01MH108579 to T.M., 1DP2HD083992 to M.D.S.]; Helen Hay Whitney Foundation [to D.C.]; Searle Scholars Program [to M.D.S.]. Funding for the open access charge: National Institute of Health [1DP2HD083992 to M.D.S.].
Conflict of interest statement. None declared.

REFERENCES

- Danko,C.G., Hah,N., Luo,X., Martins,A.L., Core,L.J., Lis,J.T., Siepel,A. and Kraus,W.L. (2013) Signaling pathways differentially affect RNA polymerase II initiation, pausing, and elongation rate in cells. *Mol. Cell*, **50**, 212–222.
- Tennyson,C.N., Klamut,H.J. and Worton,R.G. (1995) The human dystrophin gene requires 16 hours to be transcribed and is cotranscriptionally spliced. *Nat. Genet.*, **9**, 184–190.
- Fuchs,G., Voichek,Y., Benjamin,S., Gilad,S., Amit,I. and Oren,M. (2014) 4sUDRB-seq: measuring genomewide transcriptional elongation rates and initiation frequencies within cells. *Genome Biol.*, **15**, R69.
- O'Brien,T. and Lis,J.T. (1993) Rapid changes in *Drosophila* transcription after an instantaneous heat shock. *Mol. Cell. Biol.*, **13**, 3456–3463.
- Darzacq,X., Shav-Tal,Y., de Turrís,V., Brody,Y., Shenoy,S.M., Phair,R.D. and Singer,R.H. (2007) In vivo dynamics of RNA polymerase II transcription. *Nat. Struct. Mol. Biol.*, **14**, 796–806.
- Saldi,T., Cortazar,M.A., Sheridan,R.M. and Bentley,D.L. (2016) Coupling of RNA polymerase II transcription elongation with pre-mRNA splicing. *J. Mol. Biol.*, **428**, 2623–2635.
- Saint-André,V., Batsché,E., Rachez,C. and Muchardt,C. (2011) Histone H3 lysine 9 trimethylation and HP1 γ favor inclusion of alternative exons. *Nat. Struct. Mol. Biol.*, **18**, 337–344.
- Veloso,A., Kirkconnell,K.S., Magnuson,B., Biewen,B., Paulsen,M.T., Wilson,T.E. and Ljungman,M. (2014) Rate of elongation by RNA polymerase II is associated with specific gene features and epigenetic modifications. *Genome Res.*, **24**, 896–905.
- Sui,W., Cao,C., W.C., J.C., W.X., P.L., Guo,L. and Y.D. (2014) Comparative analyses of histone H3K9 trimethylations in the heart and spleen of normal humans. *Genetics Mol. Res.*, **13**, 1697–1706.
- Ong,C.-T. and Corces,V.G. (2011) Enhancer function: new insights into the regulate of tissue-specific gene expression. *Nat. Rev. Genet.*, **12**, 283–293.
- Sonawane,A.R., Platig,J., Fagny,M., Chen,C.-Y., Paulson,J.N., Lopes-Ramos,C.M., DeMeo,D.L., Quackenbush,J., Glass,K. and Kuijjer,M.L. (2017) Understanding tissue-specific gene regulation. *Cell Rep.*, **21**, 1077–1088.
- Dölken,L., Ruzsics,Z., Rädle,B., Friedel,C., Zimmer,R., Mages,J., Hoffmann,R., Dickinson,P., Forster,T., Ghazal,P. *et al.* (2008) High-resolution gene expression profiling for simultaneous kinetic parameter analysis of RNA synthesis and decay. *RNA*, **14**, 1959–1972.
- Gay,L., Miller,M., Ventura,P., Devasthali,V., Vue,Z., Thompson,H., Temple,S., Zong,H., Cleary,M., Stankunas,K. *et al.* (2013) Mouse TU tagging: a chemical/genetic intersectional method for purifying cell type-specific nascent RNA. *Genes Dev.*, **27**, 98–115.
- Core,L.J., Waterfall,J.J. and Lis,J.T. (2008) Nascent RNA sequencing reveals widespread pausing and divergent initiation at human promoters. *Science*, **322**, 1845–1848.
- Tani,H., Mizutani,R., Salam,K., Tano,K., Ijiri,K., Wakamatsu,A., Isogai,T., Suzuki,Y. and Akimitsu,N. (2012) Genome-wide determination of RNA stability reveals hundreds of short-lived noncoding transcripts in mammals. *Genome Res.*, **22**, 947–956.
- Jao,C. and Salic,A. (2008) Exploring RNA transcription and turnover in vivo by using click chemistry. *Proc. Natl. Acad. Sci. U.S.A.*, **105**, 15779–15784.
- Cleary,M., Meiering,C., Jan,E., Guymon,R. and Boothroyd,J. (2005) Biosynthetic labeling of RNA with uracil phosphoribosyltransferase allows cell-specific microarray analysis of mRNA synthesis and decay. *Nat. Biotechnol.*, **23**, 232–237.
- Duffy,E.E., Rutenberg-Schoenberg,M., Stark,C.D., Kitchen,R.R., Gerstein,M.B. and Simon,M.D. (2015) Tracking distinct RNA populations using efficient and reversible covalent chemistry. *Mol. Cell*, **59**, 858–866.
- Tani,H. and Akimitsu,N. (2012) Genome-wide technology for determining RNA stability in mammalian cells: historical perspective and recent advantages based on modified nucleotide labeling. *RNA Biol.*, **9**, 1233–1238.
- Yi,X., Tesmer,V.M., Savre-Train,I., Shay,J.W. and Wright,W.E. (1999) Both transcriptional and posttranscriptional mechanisms regulate human telomerase template RNA levels. *Mol. Cell. Biol.*, **19**, 3989–3997.
- Windhanger,L., Bonfert,T., Burger,K., Ruzsics,Z., Krebs,S., Kauffmann,S., Malterer,G., L'Hernault,A., Schilhoben,M., Schreiber,S. *et al.* (2012) Ultrashort and progressive 4sU-tagging reveals key characteristics of RNA processing at nucleotide resolution. *Genome Res.*, **22**, 2031–2042.
- Schwalb,B., Michel,M., Zacher,B., Frühauf,K., Demel,C., Tresch,A., Gagneur,J. and Cramer,P. (2016) TT-seq maps the human transient transcriptome. *Science*, **352**, 1225–1228.
- Russo,J., Heck,A.M., Wilusz,J. and Wilusz,C.J. (2017) Metabolic labeling and recovery of nascent RNA to accurately quantify mRNA stability. *Methods*, **120**, 39–48.
- Li,H.-B., Tong,J., Zhu,S., Batista,P.J., Duffy,E.E., Zhao,J., Bailis,W., Cao,G., Kroehling,L., Chen,Y. *et al.* (2017) m6A mRNA methylation controls T cell homeostasis by targeting the IL-7/STAT5/SOCS pathways. *Nature*, **548**, 338–342.
- Kaech,S. and Banker,G. (2006) Culturing hippocampal neurons. *Nat. Protoc.*, **1**, 2406–2415.
- Fuchs,G., Voichek,Y., Rabani,M., Benjamin,S., Gilad,S., Amit,I. and Oren,M. (2015) Simultaneous measurement of genome-wide transcription elongation speeds and rates of RNA polymerase II transition into active elongation with 4sUDRB-seq. *Nat. Protoc.*, **10**, 605–618.

27. Gregersen, L., Schueler, M., Munschauer, M., Mastrobuoni, G., Chen, W., Kempa, S., Dieterich, C. and Landthaler, M. (2014) MOV10 is a 5' to 3' RNA helicase contributing to UPF1 mRNA target degradation by translocation along 3' UTRs. *Mol. Cell*, **54**, 573–585.
28. Zhang, B., Yang, G., Chen, Y., Zhao, Y., Gao, P., Liu, B., Wang, H. and Zheng, Z.-L. (2016) C-terminal domain (CTD) phosphatase links Rho GTPase signaling to Pol II CTD phosphorylation in *Arabidopsis* and yeast. *Proc. Natl. Acad. Sci. U.S.A.*, **113**, E8197–E8206.
29. Duffy, E.E. and Simon, M.D. (2016) Enriching s4U-RNA using methane thiosulfonate (MTS) chemistry. *Curr. Protoc. Chem. Biol.*, **8**, 234–250.
30. Dobin, A., Davis, C.A., Schlesinger, F., Drenkow, J., Zaleski, C., Jha, S., Batut, P., Chaisson, M. and Gingeras, T.R. (2013) STAR: ultrafast universal RNA-seq aligner. *Bioinformatics*, **29**, 15–21.
31. Kersey, P., Allen, J., Christensen, M., Davis, P., Falin, L., Grabmueller, C., Hughes, D., Humphrey, J., Kerhornou, A., Khobova, J. *et al.* (2014) Ensembl Genomes 2013: scaling up access to genome-wide data. *Nucleic Acids Res.*, **42**, D546–D552.
32. McDowall, M.D., Harris, M.A., Lock, A., Rutherford, K., Staines, D.M., Bähler, J., Kersey, P.J., Oliver, S.G. and Wood, V. (2015) PomBase 2015: updates to the fission yeast database. *Nucleic Acids Res.*, **43**, D656–D661.
33. Anders, S., Pyl, P.T. and Huber, W. (2015) HTSeq—a Python framework to work with high-throughput sequencing data. *Bioinformatics*, **31**, 166–169.
34. Mi, H., Muruganujan, A. and Thomas, P.D. (2013) PANTHER in 2013: modeling the evolution of gene function, and other gene attributes, in the context of phylogenetic trees. *Nucleic Acids Res.*, **41**, D377–D386.
35. Ernst, J., Kheradpour, P., Mikkelsen, T.S., Shoresh, N., Ward, L.D., Epstein, C.B., Zhang, X., Wang, L., Issner, R., Coyne, M. *et al.* (2011) Mapping and analysis of chromatin state dynamics in nine human cell types. *Nature*, **473**, 43–49.
36. Liu, Q., Wang, J., Zhao, Y., Li, C.-I., Stengel, K.R., Acharya, P., Johnston, G., Hiebert, S.W. and Shyr, Y. (2017) Identification of active miRNA promoters from nuclear run-on RNA sequencing. *Nucleic Acids Res.*, **45**, e121.
37. Stroud, H., Su, S.C., Hrvatin, S., Greben, A.W., Renthal, W., Boxer, L.D., Nagy, M.A., Hochbaum, D.R., Kinde, B., Gabel, H.W. *et al.* (2017) Early-Life gene expression in neurons modulates lasting epigenetic states. *Cell*, **171**, 1151–1164.
38. Langmead, B. and Salzberg, S. (2012) Fast gapped-read alignment with Bowtie 2. *Nat. Methods*, **9**, 357–359.
39. Zhang, Y., Liu, T., Meyer, C.A., Eeckhoutte, J., Johnson, D.S., Bernstein, B.E., Nusbaum, C., Myers, R.M., Brown, M., Li, W. *et al.* (2008) Model-based analysis of ChIP-Seq (MACS). *Genome Biol.*, **9**, R137.
40. Miller, C., Schwalb, B., Maier, K., Schulz, D., Dümcke, S., Zacher, B., Mayer, A., Sydow, J., Marcinowski, L., Dölken, L. *et al.* (2011) Dynamic transcriptome analysis measures rates of mRNA synthesis and decay in yeast. *Mol. Syst. Biol.*, **4**, 458.
41. Rabani, M., Levin, J.Z., Fan, L., Adiconis, X., Raychowdhury, R., Garber, M., Gnirke, A., Nusbaum, C., Hacohen, N., Friedman, N. *et al.* (2011) Metabolic labeling of RNA uncovers principles of RNA production and degradation dynamics in mammalian cells. *Nat. Biotechnol.*, **29**, 436–442.
42. Fossom, L.H., Sterling, C.R. and Tank, W.A. (1992) Regulation of tyrosine hydroxylase gene transcription rate and tyrosine hydroxylase mRNA stability by cyclic AMP and glucocorticoid. *Mol. Pharmacol.*, **42**, 898–908.
43. Zeiner, G.M., Cleary, M.D., Fouts, A.E., Meiring, C.D., Mocarski, E.S. and Boothroyd, J.C. (2008) In: Wilusz, J. (ed). *Post-Transcriptional Gene Regulation. Methods in Molecular Biology*. Humana Press, Vol. **419**.
44. Yang, E., van Nimwegen, E., Zavolan, M., Rajewsky, N., Schroeder, M., Magnasco, M. and Darnell, J.E.J. (2003) Decay rates of human mRNAs: correlation with functional characteristics and sequence attributes. *Genome Res.*, **13**, 1863–1872.
45. Friedel, C.C., Dolken, L., Ruzsics, Z., Koszinowski, U. and Zimmer, R. (2009) Conserved principles of mammalian transcription regulation revealed by RNA half-life. *Nucleic Acids Res.*, **37**, e115.
46. Peltz, S.W. and Ross, J. (1987) Autogenous regulation of histone mRNA decay by histone proteins in a cell-free system. *Mol. Cell Biol.*, **7**, 4345–4356.
47. Schofield, J.A., Duffy, E.E., Kiefer, L., Sullivan, M.C. and Simon, M.D. (2018) TimeLapse-seq: adding a temporal dimension to RNA sequencing through nucleoside recoding. *Nat. Methods*, **15**, 221–225.
48. Michel, M., Demel, C., Zacher, B., Schwalb, B., Krebs, S., Blum, H., Gagneur, J. and Cramer, P. (2017) TT-seq captures enhancer landscapes immediately after T-cell stimulation. *Mol. Syst. Biol.*, **13**, 920.
49. Core, L.J., Martins, A.L., Danko, C.G., Waters, C., Siepel, A. and Lis, J.T. (2014) Analysis of nascent RNA identifies a unified architecture of initiation regions at mammalian promoters and enhancers. *Nat. Genet.*, **46**, 1311–1320.
50. Hua, X., Chen, L., Wang, J., Li, J. and Wingender, E. (2016) Identifying cell-specific microRNA transcriptional start sites. *Bioinformatics*, **32**, 2403–2410.
51. Jonkers, I., Kwak, H. and Lis, J.T. (2014) Genome-wide dynamics of Pol II elongation and its interplay with promoter proximal pausing, chromatin, and exons. *eLIFE*, **3**, e02407.
52. Jonkers, I. and Lis, J.T. (2015) Getting up to speed with transcription elongation by RNA polymerase II. *Nat. Rev. Mol. Cell Biol.*, **16**, 167–177.
53. Steger, D.J., Lefterova, M.I., Ying, L., Stonestrom, A.J., Schupp, M., Zhuo, D., Vakoc, A.L., Kim, J.-E., Chen, J., Lazar, M.A. *et al.* (2008) DOT1L/KMT4 Recruitment and H3K79 methylation are ubiquitously coupled with gene transcription in mammalian cells. *Mol. Cell Biol.*, **28**, 2825–2839.
54. Gallo, J.-M., Jin, P., Thornton, C.A., Lin, H., Robertson, J., D'Souza, I. and Schlaepfer, W.W. (2005) The role of RNA and RNA processing in neurodegeneration. *J. Neurosci.*, **25**, 10372–11375.
55. Consortium, E.P. (2012) An integrated encyclopedia of DNA elements in the human genome. *Nature*, **489**, 57–74.